**Ocean Science**

# Influence of numerical schemes on current-topography interactions in 1/4° global ocean simulations

**T. Penduff**[1], **J. Le Sommer**[1], **B. Barnier**[1], **A.-M. Treguier**[2], **J.-M. Molines**[1], and **G. Madec**[3]

[1]Laboratoire des Ecoulements Géophysiques et Industriels, CNRS, UJF, INPG, Grenoble, France
[2]Laboratoire de Physique des Océans, CNRS, UBO, IFREMER, Brest, France
[3]Laboratoire d'Océanographie et de Climat par Expérimentation et Approche Numérique, CNRS, UPMC, IRD, MNHN, Paris, France

**Abstract.** The combined use of partial steps and of an energy-enstrophy conserving momentum advection scheme was shown by Barnier et al. (2006) to yield substantial improvements in the surface solution of the DRAKKAR $\frac{1}{4}°$ global sea-ice/ocean model. The present study extends this investigation below the surface with a special focus on the Atlantic and reveals many improvements there as well: e.g. more realistic path, structure and transports of major currents (Gulf Stream, North Atlantic Current, Confluence region, Zapiola anticyclone), behavior of shedded rings, narrower subsurface boundary currents, stronger mean and eddy flows (MKE and EKE) at depth, beneficial enhancement of cyclonic (anticyclonic) flows around topographic depressions (mountains). Interestingly, adding a no-slip boundary condition to this improved model setup cancels most of these improvements, bringing back the biases diagnosed without the improved momentum advection scheme and partial steps (these biases are typical of other models at comparable or higher resolutions). This shows that current-topography interactions and full-depth eddy-admitting model solutions can be seriously deteriorated by near-bottom sidewall friction, either explicit or inherent to inadequate numerical schemes.

## 1 Introduction

The three main types of Ocean General Circulation Models essentially differ by their vertical coordinate system (Griffies et al., 2000): geopotential coordinates (in so-called z-level models) and terrain-following coordinates (in so-called sigma models) remain fixed in time, while isopycnic coordinates follow density surfaces in time. More recent hybrid coordinates aim at taking advantage of these various approaches in specific regions. Intercomparison experiments

*Correspondence to:* T. Penduff
(thierry.penduff@hmg.inpg.fr)

(e.g. Roberts et al., 1996; DYNAMO Group, 1997; Chassignet et al., 2000; Treguier et al., 2005) have contributed to improve basin-scale ocean models by a careful evaluation of their respective strengths and weaknesses. More specifically, these studies revealed that current-topography interactions are essential for the simulation of realistic ocean states, that these processes are handled differently by various classes of models, and that the increase of resolution tends to lessen the discrepancy between various solutions. The DYNAMO experiment (Willebrand et al., 2001) was focused on $\frac{1}{3}°$ (so-called eddy-admitting) ocean models able to partly resolve the mesoscale activity. Along with the ongoing (and beneficial) increase of basin- and global-scale ocean model resolution (Paiva et al., 1999; Smith et al., 2000; Eden and Böning, 2002; Masumoto et al., 2004; Chanut et al., 2007), eddy-admitting ocean models require further investigation since the $\frac{1}{4}°$ resolution is the target of future ocean climate models. In this context, important questions remain open concerning the sensitivities of such models, and the benefits of (partially) resolving oceanic eddies in future climate assessments.

The DYNAMO program revealed specific tendencies of widely-used z-level models in the eddy-admitting regime. Further investigations made during the French CLIPPER experiment (presented in Tréguier et al., 1999) highlighted additional biases in $\frac{1}{3}°$ and $\frac{1}{6}°$ eddy-admitting z-level solutions with respect to observations and sigma-coordinate solutions. It was conjectured (Penduff et al., 2002, 2005) that the robust lack of kinetic energy found at depth, possibly due to spurious topographic friction, may adversely affect current-topography interactions and explain the circulation biases found at the surface. These circulation biases (and their conjectured origin) are likely not specific to CLIPPER; they are met in other setups, other eddy-admitting and eddy-resolving models, including the first version of the $\frac{1}{4}°$ global DRAKKAR model based on CLIPPER-like numerics (Barnier et al., 2006). This latter study describes how two numerical changes (the use of partial steps and of an

**Table 1.** Differences between the four model experiments (see text). The same simulations were investigated by Barnier et al. (2006), but are renamed here for clarity.

| Simulation name in Barnier et al. (2006) | Simulation name in the present paper | Momentum advection scheme | Topography | Sidewall boundary conditions |
|---|---|---|---|---|
| ORCA025-G04 | ENSf | ENS | Full steps | Free-slip |
| ORCA025-G03 | EENf | EEN | Full steps | Free-slip |
| ORCA025-G22 | EENp | EEN | Partial steps | Free-slip |
| / | EENp-ns | EEN | Partial steps | No-slip |

enstrophy-energy-conserving momentum advection scheme) largely improved this initial DRAKKAR solution, removing a substantial part of the biases found usually in this class of model solutions and making it comparable to higher resolution standards. These improvements were especially noticed in regions of strong eddy activity and topographic influence, suggesting a beneficial modification of topographic constraints on the eddy and the mean flow.

Barnier et al. (2006) described the successive impact of both numerical changes on DRAKKAR solutions near the surface with respect to observed mean sea-surface height (Niiler et al., 2003) and altimeter-derived Eddy Kinetic Energy (EKE, Ducet et al., 2000). The present paper extends the former assessment toward the subsurface and makes use of an additional simulation to investigate the impact of momentum advection schemes, partial steps, and sidewall boundary conditions on the simulated dynamics and on current-topography interactions. We aim at complementing Barnier et al. (2006)'s study, illustrating the major role of discrete topographic constraints on the simulated dynamics, interpreting the origin of the circulation biases mentioned in CLIPPER-like models and of the improvements seen in DRAKKAR setups. A detailed investigation of certain improvements reported here and in Barnier et al. (2006) is presented from a numerical point of view in Le Sommer et al. (2007). The numerical setup and the four sensitivity experiments are presented in Sect. 2. The sensitivity of the model to changes in the momentum advection scheme and to the use of partial steps in then described, with a focus on circulation features (Sect. 3), on the vertical structure of the flow and topographic constraints (Sect. 4). Section 5 discusses the impact of sidewall boundary conditions and sheds light on the former results. Our results are summarized and discussed in Sect. 6.

## 2 Model, configurations, experiments

The reader is referred to Barnier et al. (2006) for a complete description of the global $\frac{1}{4}°$ model setup: only the main features are recalled here. This configuration (ORCA025) is part of the DRAKKAR hierarchy of models (DRAKKAR

Group, 2007), developed by a consortium of several research groups in Europe and with the Mercator-Ocean Operational Oceanography Reasearch and Development Team. This global sea-ice ocean model, implemented here on a 46-level $\frac{1}{4}°$-resolution tripolar ORCA grid, is based on the NEMO modeling system[1] which includes the z-coordinate free-surface ocean code OPA9 and the multi-layered sea-ice code LIM2. The simulations presented here use a Flux Corrected Transport (FCT) scheme (Lévy et al., 2001) for tracer advection. Climatological initial conditions for temperature and salinity are taken in January from PHC2.1 (Steele et al., 2001) at high latitudes, MEDATLAS (Jourdan et al., 1998) in the Mediterranean, and Levitus et al. (1998) elsewhere. The 10-year simulations presented here were forced through bulk formulae by a climatological seasonal forcing without any relaxation of sea-surface temperature (SST) or salinity (SSS). These climatological atmospheric fields, close to those used by Timmermann et al. (2005) and labeled "DRAKKAR forcing set 1", combine wind stresses from ERS and NCEP, daily air temperature from NCEP/NCAR reanalysis, monthly precipitations from CMAP (Xie and Arkin, 1997), air humidity from Trenberth et al. (1989), cloud cover from Berliand and Strokina (1980), and river runoff derived from the UNESCO database (E. Rémy, personal communication).

This paper investigates the model sensitivity to various numerical parameters from four simulations (see Table 1) which share the following parameterizations :

– Laplacian isopycnal tracer diffusion is applied with a coefficient that decreases poleward proportionally to the grid size ($300 \, \mathrm{m^2 \, s^{-1}}$ at the equator).

– Momentum is dissipated horizontally at small scales by a biharmonic viscosity operator: $-1.5 \times 10^{11} \, \mathrm{m^4 \, s^{-1}}$ at the equator and decreasing poleward as the cube of the grid size. Unresolved turbulent processes exert a lateral viscosity along the equator and are parameterized over the upper $100 \, \mathrm{m}$ by an additional laplacian operator ($500 \, \mathrm{m^2 \, s^{-1}}$, see Arhan et al., 2006).

---

[1] http://www.lodyc.jussieu.fr/NEMO/

- Surface boundary layer mixing and interior vertical mixing are parameterized by a 1.5-order turbulent closure model (Blanke and Delecluse, 1993). Background vertical diffusion is set to $10^{-5}\,\mathrm{m}^2\,\mathrm{s}^{-1}$. Background vertical viscosity $K^v$ is set to $10^{-4}\,\mathrm{m}^2\,\mathrm{s}^{-1}$. In case of static instability, vertical viscosity and diffusivity are raised to $10\,\mathrm{m}^2\,\mathrm{s}^{-1}$.

- Quadratic bottom friction is introduced as a boundary stress with a simple parameterization of the effect of residual tidal currents (Willebrand et al., 2001):
  $K^v\frac{\partial u}{\partial z}=C_d\cdot\underline{u}\cdot\sqrt{(u^2+u_0^2)}$ at the bottom, with $C_d=10^{-3}$
  as in Treguier (1992), and $u_0=5\,\mathrm{cm}\,\mathrm{s}^{-1}$.

Various momentum advection schemes (MASs) are available in NEMO-OPA9. In an idealized non-divergent shallow water framework, the horizontal components of the schemes referred to as ENS (Sadourny, 1975) and EEN (Arakawa and Lamb, 1981) conserve potential enstrophy and both energy and potential enstrophy, respectively. The conservation of potential enstrophy is not ensured in the present realistic case. These latter studies show that imposing constraints on the momentum advection scheme truncation error significantly improves the solutions obtained in marginally resolved regimes, e.g. the present eddy-admitting case. In particular, Arakawa and Lamb (1981) show that energy and potential enstrophy conservation suppresses a spurious energy cascade found in the presence of steep topography when only enstrophy is conserved. Both ENS and EEN schemes are written in the vector-invariant form; an extensive description of their formulations and of their dynamical behavior in a realistic setting similar to ours is given in Le Sommer et al. (2007). Simulations ENSf and EENf (see Table 1) will be compared to each other to evaluate the dynamical impact of momentum advection schemes.

Topography is represented as staircases in all runs. It is distorted in the cases when local depths are approximated to the closest model level (i.e. full steps, simulations ENSf and EENf), and much less with partial steps (Pacanowski and Gnanadesikan, 1998) where the thickness of bottom grid cells is adjusted to the real depth (simulations EENp and EENp-ns). Topography representation is the only difference between EENf and EENp that will thus be compared to study the global impact of partial steps. Note that the CLIPPER simulations were performed with the ENS scheme and full step topographies (like the present ENSf run). The present study, along with those by Barnier et al. (2006) and Le Sommer et al. (2007), describe the impact of these new choices in DRAKKAR models, and contributes to explain the improvements between CLIPPER and DRAKKAR solutions.

The first three runs listed in Table 1 were performed with free-slip boundary conditions. The impact of sidewall friction in the eddy-admitting regime will be evaluated by comparing EENp to EENp-ns, this latter run differing only from the former by a no-slip boundary condition (see Table 1). Un-
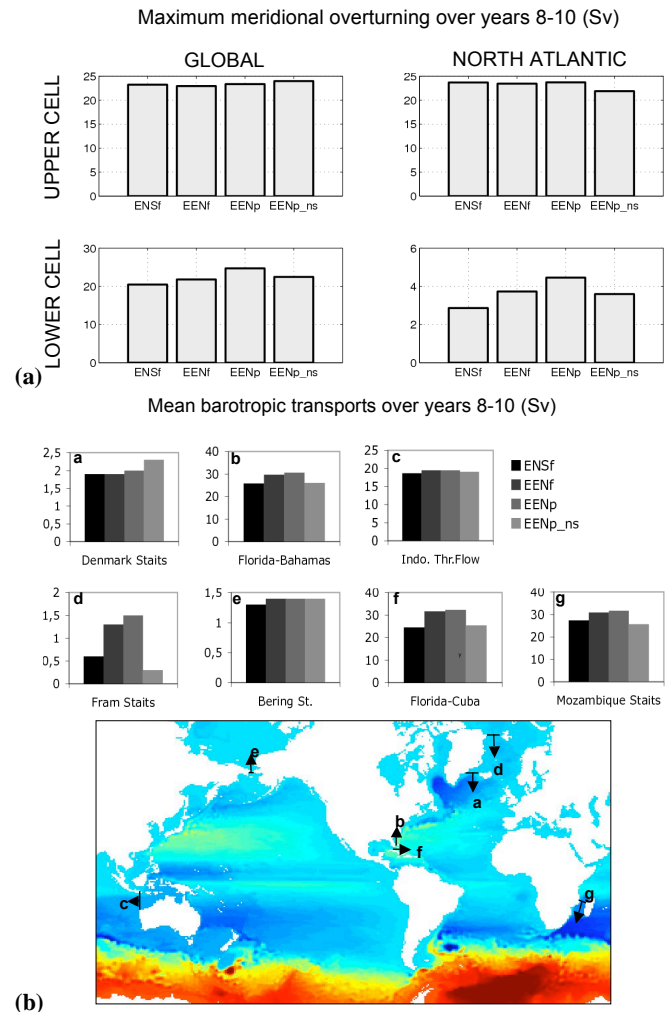


**Fig. 1.** **(a)** Maximum intensity of the meridional overturning streamfunctions (Sv) computed in z-coordinates over years 8–10 of the four simulations in the northern hemisphere; shown for the upper and lower cells (upper and lower plots) of the global (left column) and Atlantic (right column) basins. **(b)** Barotropic transports at 7 straits (see map) in the four simulations averaged over years 8–10.

less stated otherwise, the four simulations will be compared in the following in terms of averages and variances of various quantities computed from the last three years (8 to 10) of 10-year integrations.

## 3 Momentum advection and topography: circulation features

The path and structure of simulated horizontal currents respond quickly to modified numerics, i.e. within about 1 year. Modified advection might then make the three simulations diverge in terms of T-S structure; indeed this becomes

**Table 2.** Summary of the model sensitivity in the Atlantic (see text and Figs. 2, 3, 4, 6).

| | ENSf → EENf<br>ENS → EEN | EENf → EENp<br>F. steps → P. steps | EENp → EENp-ns<br>Free-slip → No-slip |
|---|---|---|---|
| Transport of<br>Labrador Current | ~40 Sv → ~50 Sv | ~50 Sv → ~60 Sv | ~60 Sv → ~40 Sv |
| Northwest Corner | Appears | Remains present | Disappears |
| GS: Northern<br>Recirculation<br>Gyre | ~10 Sv → ~20 Sv | ~20 Sv → ~30 Sv | ~30 Sv → ~0 Sv |
| GS: Southern<br>Recirculation<br>Gyre | Very local, ~10 Sv<br>→<br>Local, ~20 Sv | Local, ~20 Sv<br>→<br>Elongated, ~30 Sv | Elongated, ~30 Sv<br>→<br>Very local, ~10 Sv |
| Deep Western<br>Boundary Current<br>off Brazil | Weak eddies appear | Stronger eddies | Weaker eddies |
| Transport of<br>Zapiola Anticyclone | ~0 Sv → ~0 Sv | ~0 Sv → ~200 Sv | ~200 Sv → ~100 Sv |
| Northernmost<br>latitude of<br>Malvinas Current | 39° S → 34° S | 34° S → 34° S | 34° S → 39° S |
| Behavior of<br>Agulhas Rings | More dispersion<br>More zonal drift | Less dispersion | EENp-ns similar<br>to ENSf |

noticeable after about 5 years. On even longer timescales, SST distributions might have diverged enough to affect the surface buoyancy forcing (despite unchanged atmospheric variables) through bulk formulae, and eventually the meridional overturning circulation. Our 10-year integrations are too short to study the ultimate impact of these numerical changes, but well suited to study how various numerical choices establish different (and persistent) circulation patterns. This section is focused on the sensitivity of the flow at different depths to the change of MAS and topographic representation.

## 3.1 Meridional overturning circulation and horizontal transports

Figure 1a shows for the Global and Atlantic Oceans the maximum intensity of the upper and lower cells of the MOC. The magnitude of the upper (lower) cell quantifies the northward transport of warm surface (cold bottom) waters; in the Atlantic for all simulations, these extrema are located around 37° N/1000 m and 15° N/4000 m respectively (Barnier et al., 2006, their Fig. 3). As noted in this latter paper, the upper

mean MOC averaged over the last three years of the simulation is relatively strong in our simulations (23–24 Sv), and the sensitivity of some regional circulation patterns to the model numerics might be related to this regime. Neither the MAS nor the topographic representation substantially modify the maximum intensity of the Atlantic and global upper MOCs: the extrema remain close to [35° N−1000 m] and change by less than 2%. No change of the upper meridional circulation is noticeable in the Indian and Pacific Oceans either. This supports the fact that numerically-induced circulation changes did not significantly feed back to the surface buoyancy fluxes via a large-scale change of SST advection over 10 years. On the contrary, the deep limb of the MOC (associated with the northward spreading and upwelling of Antarctic Bottom Water, AABW) is strongly affected by our numerical changes over this 10-year period. Its maxima, found around [30° S−4000 m] globally and [15/20° N−4000 m] in the Atlantic, substantially increase in the ENSf-EENf-EENp sequence: respectively +8/+28% (global/Atlantic) when ENS is replaced by EEN, and additional +11/+18% when partial steps are used. An increase of the deep MOC is observed in the Indo-Pacific Ocean as well.

Both numerical changes thus induce a direct enhancement of the deep circulation in the Global Ocean.

Figure 1b shows the depth-integrated time-averaged transports at choke points in ENSf, EENf and EENp simulations. These transports increase when the ENS MAS is replaced by EEN (ENSf vs. EENf), and, to a lesser extent, when the full step topography is replaced by partial steps (EENf vs. EENp). The currents across Florida-Bahamas, Florida-Cuba, and Mozambique Straits (labeled a, b, c in Fig. 1b) mainly carry upper-layer waters poleward, part of which contribute to the upper MOC; their enhancement is not seen in the upper MOCs, suggesting that these increments recirculate horizontally.

In summary, highly-confined and deep flows get stronger with the EEN MAS, and even more so with partial steps. We may thus conjecture at this point that both numerical changes reduce the dissipation of horizontal momentum along topographies. This hypothesis is further examined below.

## 3.2 Atlantic circulation features

Since Rhines (1977)'s pioneering paper, many studies have confirmed that mesoscale eddies are produced by and interact with the general circulation, and that these non-linear eddy-mean flow interactions are highly sensitive to sloping topographies. Eddy-active regions such as western boundary currents and their eastward extensions are locations where eddy-mean flow and current-topography interactions are strong, and thus are expected to be particularly sensitive to the choice of the momentum advection scheme and the representation of topography. The impact of the EEN MAS and partial step topography, shown by Barnier et al. (2006) to be beneficial at the surface, is now investigated in more detail at depth in the Atlantic. Table 2 summarizes how both changes affect the model solution in this basin (also see Barnier et al., 2006's Figs. 5, 7 and 8).

### 3.2.1 North Atlantic

Our numerical changes do not modify the transport of Greenland-Scotland overflows, the magnitude, structure and depth of the Atlantic upper MOC, nor the transport of the Deep Western Boundary Current (DWBC, shown at 1500 m in Fig. 2 for all simulations). The structure of the DWBC is, however, modified. Between the Reykjanes Ridge and the tip of the Grand Banks, the DWBC becomes faster and narrower from ENSf to EENf, and from EENf to EENp. Poleward countercurrents are better-defined in EENf and EENp offshore the DWBC in the southwest Labrador Sea, and east of the Grand Banks. In EENf and EENp, most of the DWBC remains trapped along the topographic slope between the Grand Banks and Cape Hatteras (10–15 cm s$^{-1}$), whereas ENSf simulates a broad vein that remains away from the slope.

Mean current vectors and
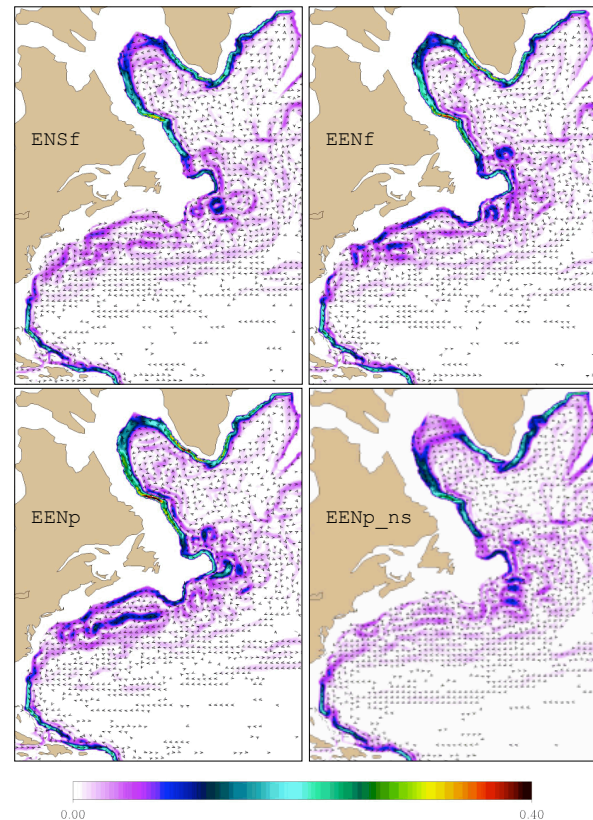speed at 1500 m (years 8-10)



**Fig. 2.** Current vectors and velocities (colors, m s$^{-1}$) at 1500 m along the northwestern boundary of the Atlantic, averaged over years 8–10 in the four simulations. Only one vector out of 16 is represented.

Figure 3 shows the vertical structure of the mean flow across the Gulf Stream (GS) and the DWBC at 69° N as measured by Joyce et al. (2005) and diagnosed from the DRAKKAR simulations. The ENSf solution is clearly unrealistic there: the GS is located too far south (around 37° N), the equatorward DWBC is wide and slow, it reaches the surface at latitudes (38° N) where the GS is actually observed, and an unrealistic shallow vein of warm water flows poleward along the American shelf. The use of the EEN scheme (EENf) does not suppress this shallow warm current, but lessens the model-observation mismatch: it confines the shallow current horizontally, the DWBC becomes a more realistic vein trapped along the topographic slope, and an eastward barotropic jet appears at the observed GS location. The addition of partial steps (EENp) does not totally suppress the shallow vein, does not help the DWBC match its observed depth range (still 700 m too shallow) and maximum velocities reach their observed magnitudes in the near-surface GS (50 cm/s instead of 80) and in the DWBC (about 10 cm/s instead of 30). However, the EENp solution highlights major
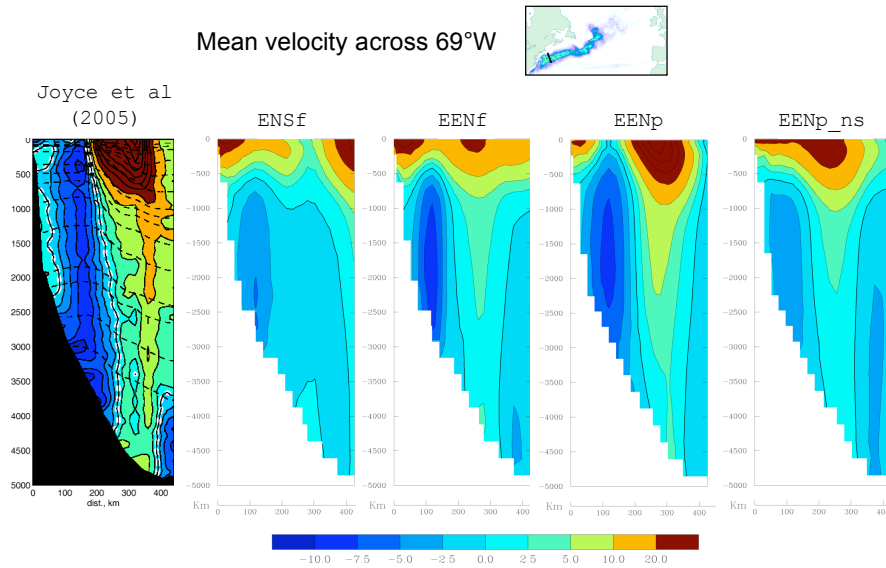
**Fig. 3.** Mean normal velocity across the 69° N section shown on top, derived from current meter measurements (Joyce et al., 2005) and averaged over years 8–10 from the four simulations. Contour intervals: $5\,\mathrm{cm\,s^{-1}}$ below $-10\,\mathrm{cm\,s^{-1}}$, like color limits between $-10$ and $+20\,\mathrm{cm\,s^{-1}}$, $10\,\mathrm{cm\,s^{-1}}$ above $+20\,\mathrm{cm\,s^{-1}}$. The zero contour is highlighted in white and black in the observations and simulations, respectively.

improvements from surface to bottom: the GS becomes a surface-intensified front with realistic structure and location, the intensity of the shallow vein is subtantially reduced, and the DWBC remains at a correct location.

Most of the poleward flow within the NAC steers around the quasi-stationary Northwest Corner before heading toward the eastern North Atlantic. This anticyclonic circulation is weak in the ENSf solution and appears at the observed location in EENf and EENp (44 ° W, 51° N). The Northwest Corner transport reaches only half of Lazier (1994)'s 50 Sv estimate (Figs. 4, Table 2), probably because the resolution remains too modest to favour strong recirculations. The deep signatures of the separated GS (Fig. 2), the shape and intensity of its Northern and Southern Recirculation Gyres (NRG and SRG) also get increasingly realistic in the sequence ENSf-EENf-EENp (Fig. 4, Table 2). Both recirclation gyres in EENp are remarkably close to those described in Dengg et al. (1996)'s review, in terms of location, shape, and internal structure (sub-gyres). These recirculation gyres have realistic transports of about 30 Sv, but two local asymmetries (NRG stronger than SRG, and southward shift of the GS velocity maximum with increasing depth) are not simulated there. Frolov et al. (2004) showed from idealized numerical experiments that in presence of a sloping topography, the observed tilt of the GS velocity maximum in the meridional-vertical plane induces an asymmetric mixing of sub-thermocline potential vorticity mixing that enhances the NRG. The simultaneous absence of both asymmetries in EENp is consistent with such a dynamical link.

A basin-scale section of EKE was done along 48° N by

Colin de Verdière et al. (1989) in the North Atlantic and is superimposed on its model counterparts in Fig. 5. The western part of the section intersects the poleward NAC where the EKE increases in the sequence ENSf-EENf-EENp. The EKE minimum observed right above the MAR, clearly absent from ENSf, is correctly reproduced in EENp. The surface-trapped EKE associated with the NAC extension east the Mid-Atlantic Ridge (MAR) is slightly better reproduced (more intense) in EENp. To sum up, the use of EEN and partial steps largely improve the mean circulation and associated eddy field throughout the northwestern Atlantic up to the surface, where their patterns tend toward those obtained at much higher resolution (see Barnier et al., 2006).

### 3.2.2    South Atlantic

ENSf, EENf and EENp simulate quite comparable DWBC's south of the GS region until about 8° N where the observed DWBC breaks up into coherent eddies (Dengler et al., 2004). Successful simulations of this transition have required horizontal resolutions of at least 1/6° so far, like in CLIPPER, up to 1/12° in the FLAME model (Dengler et al., 2004). Fig. 6 shows that the DWBC remains laminar with the ENS scheme, but generates eddies with the EEN scheme. Despite the modest resolution, the addition of partial steps improves the solution and brings EENp's eddies close to those simulated by the 1/12° FLAME model in terms of coherence, temperature anomaly (0.2°C), quasi-circular shape, mutual spacing, and size.

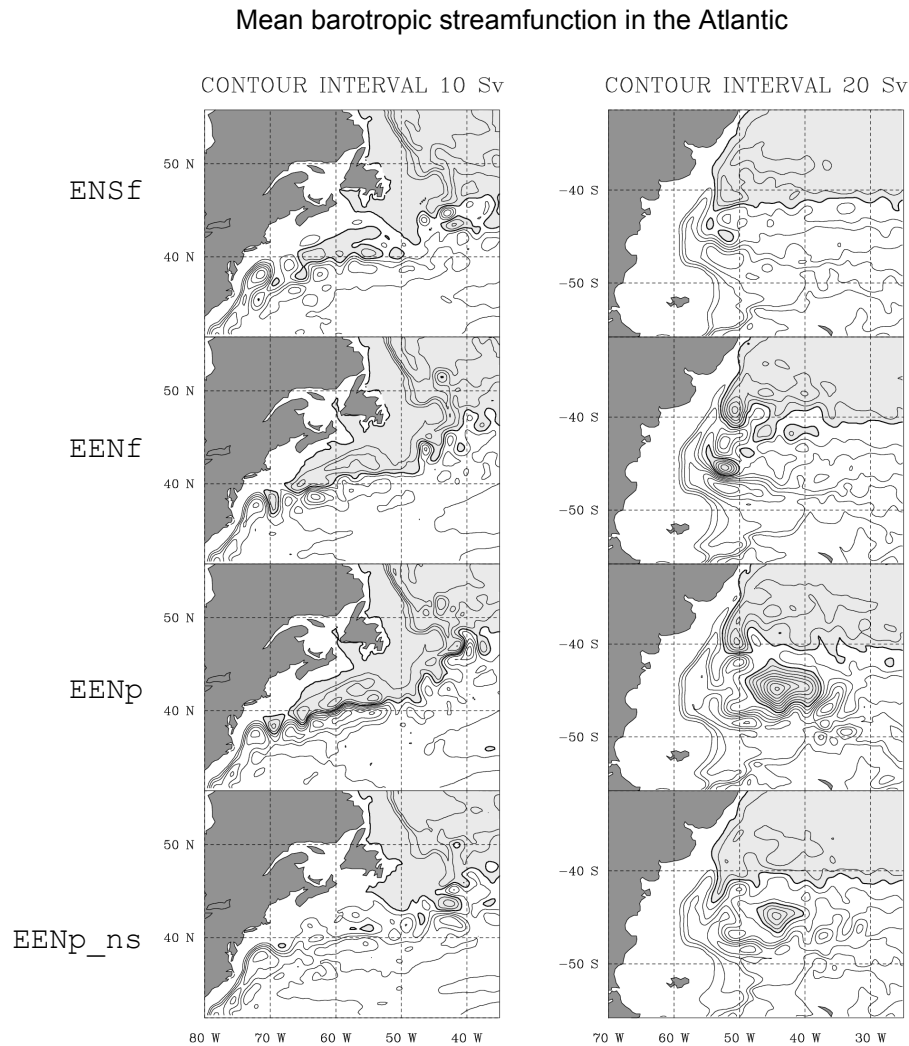## Mean barotropic streamfunction in the Atlantic



**Fig. 4.** Mean barotropic streamfunction in the Gulf Stream region (left) and in the Confluence region (right) from simulations ENSf, EENf, EENp, EENp-ns (from top to bottom). Anticlockwise circulations are shaded. Contour interval is 10 Sv (20 Sv) in the left (right) columns.

The right panels in Fig. 4 (also see Table 2 here, and Fig. 9 in Barnier et al., 2006) highlight in the Confluence region the two-step improvement of the model solution in the sequence ENSf-EENf-EENp. The EEN advection scheme enhances by 5° the northward excursion of the Malvinas Current (which reaches about 34° S, consistently with Olson et al., 1988) and intensifies stationary recirculations between 50 and 55° W. The use of partial steps further improves the solution with the appearance around [45° W, 45° S] of the eddy-driven topographically-trapped Zapiola anticyclone (De Miranda et al., 1999). Its simulated shape, mean transport (~200 Sv), surface signature and impact on the EKE field (see Barnier et al., 2006) get in very good agreement with observations. Eddy-mean flow interactions with topography play a major role in other regions such as the Cape basin (impact of the Walvis Ridge on the Agulhas Rings,

see Kamenkovich et al., 1996; Beismann et al., 1999; Penduff et al., 2002). The combined use of the EEN advection scheme and partial steps led to substantial improvements there as well (Table 2; Barnier et al., 2006).

## 4 Momentum advection and topography: vertical structure of the flow

Our changes in numerical schemes modify the vertical structure of the mean and eddy flow. These changes are described hereafter, first in terms of orientation of the mean circulation with respect to topography, then in terms of intensity of horizontal and vertical (mean and eddy) velocities.
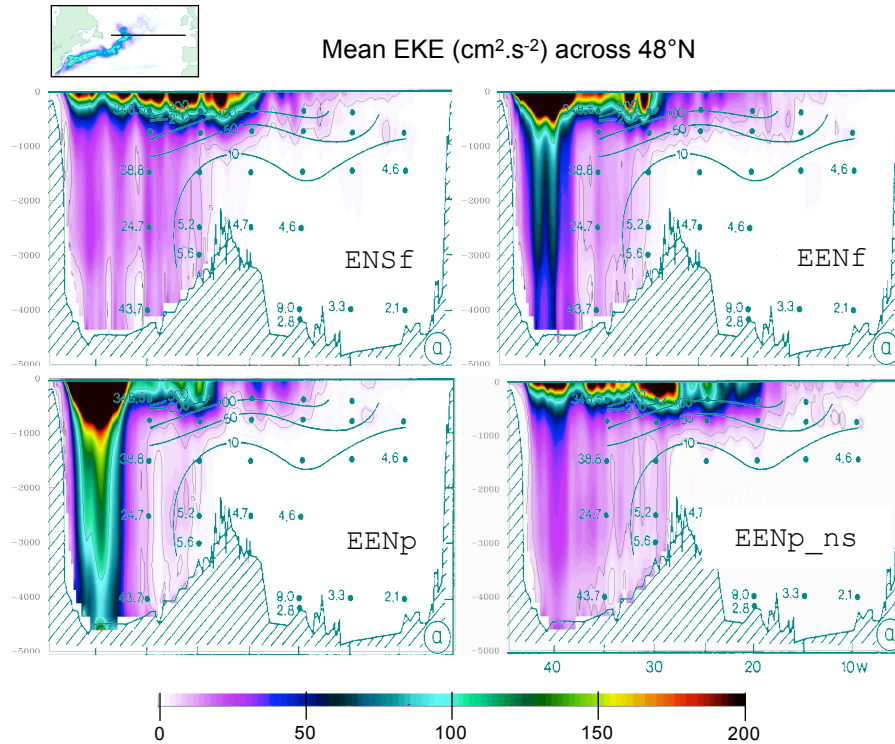
**Fig. 5.** Eddy kinetic energy section in the Atlantic across 48° (cm$^2$ s$^{-2}$) from the four DRAKKAR simulations (color) and from the current-meter measurements by Colin de Verdière et al. (1989) (contours).

## 4.1 Direction of the mean flow: topostrophy

Eddy flows interact with the ambient barotropic potential vorticity field $\frac{f}{H}$ whose gradient is influenced by sloping topographies: cross-$\frac{f}{H}$ eddy flows basically induce a downgradient, turbulent flux of barotropic potential vorticity. This nonlinear process is able to generate mean barotropic flows, such as the Zapiola Anticyclone (Dewar, 1998), which keep deep waters to the left (right) in the northern (southern) hemisphere, i.e. in the direction of $\mathbf{u}^{\text{topo}} = -\mathbf{f} \times \nabla H$. Statistical theories also predict the existence of such mean barotropic flows driven by eddy-topography interactions (Holloway, 1992). Topostrophy (Merryfield and Scott, 2007) is a statistical measure of the alignment at every cell $m$ of mean normalized currents vectors $\mathbf{u}_m$ ($|\mathbf{u}_m| = 1, \forall m$) with the barotropic circulation $\mathbf{u}_m^{\text{topo}}$. Topostrophy $T_s(x, y)$ was computed globally from years 8–10 of the four DRAKKAR simulations and binned in classes of total depth $H_j$ and level depth $d_k$ to yield $T_s(H_j, d_k)$ as done by Merryfield and Scott (2007) (unsmoothed velocity and topography, weighting $= |\nabla H|.|f|$ according to their notation):

$$T_s(H_j, d_k) = \frac{\sum_m (\mathbf{u}_m . \mathbf{u}_m^{\text{topo}}) . \delta_{jk,m} . dV_m}{\sum_m |f \nabla H|_m . \delta_{jk,m} . dV_m}, \qquad (1)$$

where $dV_m$ is the grid cell volume, $\delta_{jk,m}$ equals 1 where the bottom depth is $H_j$ and the level depth is $d_k$, 0 other-

wise. For each $(H, d)$ class, $T_s = 1$, $T_s = -1$, and $T_s = 0$ respectively correspond to simulated flows everywhere in the direction of $\mathbf{u}^{\text{topo}}$, opposite to $\mathbf{u}^{\text{topo}}$, and uncorrelated with $\mathbf{u}^{\text{topo}}$. The closer $T_s$ to unity, the more the simulated currents circulate in the direction mentioned above, and the better the model agrees with topographic rectification theories. Merryfield and Scott (2007) examined topostrophies computed from global simulations performed at various resolutions (1°, 2°, 0.4°, and 0.1°). The large difference found between coarse and fine resolution topostrophies supports the aforementioned theory, i.e. mesoscale turbulence tends to align mean currents in the direction of $\mathbf{u}^{\text{topo}}$, with values of $T_s$ increasing toward the bottom in all total depth classes.

Global topostrophies $T_s(H, d)$ are shown in Fig. 7 for the four DRAKKAR simulations. Within most depth ranges in ENSf, EENf and EENp, $T_s$ is positive and monotonically increases toward the bottom: simulated currents increasingly tend to align in the direction of topographic Rossby waves with increasing depth. $T_s$ in EENf is about twice its typical value in ENSf, over a 1000m-thick bottom layer (especially within the 0–2000 m bottom depth range). The EEN advection scheme substantially enhances $T_s$ near the surface as well. The effect of partial steps is qualitatively comparable but weaker: this further enhances deep values of $T_s$ in the 2000–4000 m bottom depth range. As a result, $T_s$ in EENp becomes rather uniform over the bottommost 1000 m
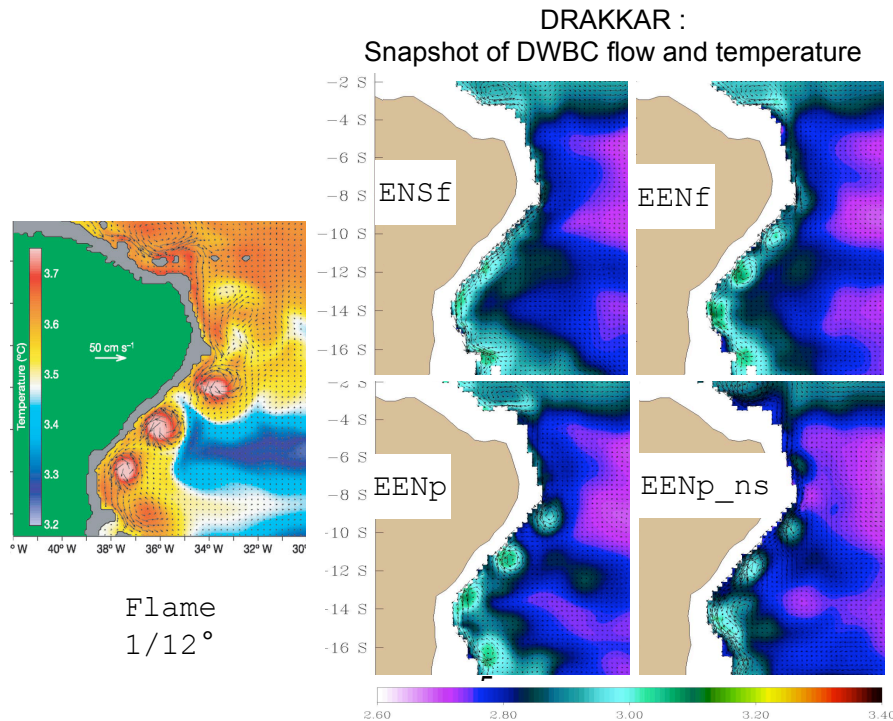
**Fig. 6.** Deep Western Boundary Current temperature and velocity snapshots in the four DRAKKAR simulations at 2500 m (22 July of year 10) and in a 1/12° FLAME simulation at 1900 m (Dengler et al., 2004).

within the 0–3500 m bottom depth range. As compared to Merryfield and Scott (2007)'s Fig. 7, the $T_s$ pattern in ENSf shares some similarities (weak values becoming negative in deep regions) with those derived from non-eddying models; our numerical changes, especially the EEN scheme, make the topostrophy structure more comparable to those derived from 0.1°models (stronger, positive almost everywhere, homogeneous within a bottommost 1000 m-thick layer). As discussed by Merryfield and Scott (2007), results of this kind do not demonstrate that eddy-topography interactions in ENSf and EENp are responsible for the changes in $T_s$, but they are strongly suggestive of such an effect.

## 4.2 Vertical structure of horizontal mean and eddy velocities

The temporal average $u$ and standard deviation $u'$ of horizontal velocity magnitudes were computed at every gridpoint over years 8–10 of each run and averaged quasi-zonally on the model grid ($j$=constant lines) to build meridional sections; these averages are noted $|u|$ and $|u'|$ respectively. Their relative differences between ENSf and EENf and between EENf and EENp are expressed in % in Fig. 8. Replacing the ENS scheme by the EEN scheme leads to a clear enhancement of mean deep velocities, especially at mid-latitudes (roughly 30–60°) in both hemispheres. The change of momentum advection scheme increases sub-thermocline mean

velocities by about 10 to 100% at the bottom in these latitude bands (+20% up to 45% on global average). This sensitivity, investigated in detail by Le Sommer et al. (2007), is particularly clear in eddy-active regions influenced by bottom topography. A similar enhancement occurs on subthermocline eddy velocities $|u'|$ as well, but to a lesser extent (about +10% in slightly narrower latitude bands). The right panels in Fig. 8 show that the addition of partial steps reinforces the deep mean and eddy flows, in a similar but stronger and more homogeneous way: everywhere north of 60° S including low latitudes, subthermocline mean (eddy) velocities increase by 10–50 (10–30)% up to 100% near the bottom.

Most circulation biases of the ENSf solution (mislocated currents, no Zapiola anticyclone, overshoot and/or spreading of western boundary currents, straight path of Agulhas eddies as mentioned in Table 2, etc.) were found in the 1/3° and 1/6° CLIPPER model solutions; they are in fact typical of many eddy-admitting and eddy-resolving ocean models (see Barnier et al., 2006). Both CLIPPER models cited above share the ENSf numerics (ENS, full steps); mean and eddy velocities were proven much too weak at depth in CLIPPER with respect to WOCE current meter data (Penduff et al., 2002, 2005). The sub-thermocline velocity increases induced by the EEN scheme and further by the partial steps are thus beneficial.
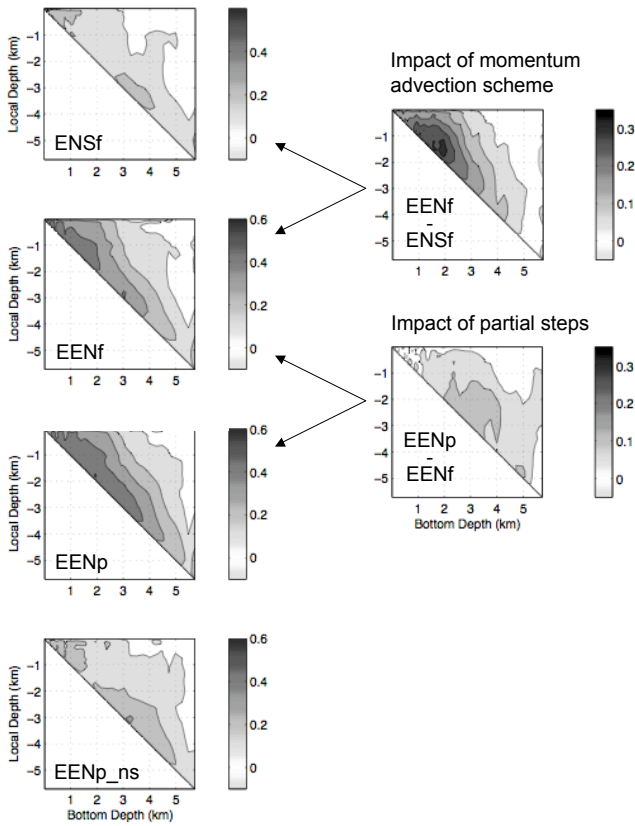
**Fig. 7.** Left: global topostrophy $T$ (see text) from simulations ENSf, EENf, EENp and EENp-ns. Right: differences $T_{EENf} - T_{ENSf}$ (impact of momentum advection scheme) and $T_{EENp} - T_{EENf}$ (impact of partial steps).

With the exception of the bottom left panel, Fig. 8 shows that the enhancement of $|u|$ and $|u'|$ due to EEN and to partial steps strongly increases with depth. It is interesting to note also that at the surface, where Barnier et al. (2006) compared these results with observations, the modifications in mean and eddy velocities induced by both numerical changes are actually aligned with those occuring below the thermocline, and much weaker than their near-bottom expressions. Eddy velocities also tend to change in the depth and latitude ranges where mean velocities do so. All these remarks strongly suggest, again, that the realism of surface mean and eddy flows in EENp are a consequence of more intense currents (and more consistent dynamics, see previous section) at depth. This explanation is consistent with a numerically-induced modification of mutual interactions between the mean flow, the eddy flow, and topography.

### 4.3 Vertical structure of vertical mean and eddy velocities

Figure 9a shows the temporal average and standard deviation of vertical velocities just above topography in EENf and EENp in the Cape Basin (the following remains true

in other eddy-active regions). The use of partial steps reduces the extrema of both statistical moments, which appear much smoother at the bottom. The mean ($|w|$) and standard deviation ($|w'|$) of vertical velocities were averaged along the model grid ($j$=constant lines) as $|u|$ and $|u'|$ introduced earlier, and are shown in Fig. 9b. Between about 500 and 4000 m at mid latitudes, the use of partial steps enhances $|w|$ and $|w'|$ by about 10–20%; these increases are collocated with their counterparts in $|u|$ and $|u'|$, respectively. Below 4000 m, partial steps enhance horizontal velocities but substantially reduce mean and eddy vertical velocities ($-30\%$ and $-15\%$ respectively) on global average at all latitudes. Partial steps thus keep the vertical-to-horizontal "aspect ratios" of mean and eddy velocities unchanged above about 4000 m, but strongly reduce them near the bottom (by 50 and 30%, respectively for $|w|/|u|$ and $|w'|/|u'|$).

Topographic slopes, especially weak ones, are much better represented with partial steps: this suppresses localized straircases where bottom $w$ and $w'$ reach their maxima in the full step case (Fig. 9a). This benefit was mentioned by Pacanowski and Gnanadesikan (1998) (their Fig. 7) and is confirmed here at higher resolution in a global realistic setup. By reducing velocity gradients at grid-scale, partial steps are expected to reduce the explicit dissipation of momentum (and vorticity) and may promote stronger velocities at depth as found in EENp. By improving the representation of $\frac{f}{H}$ contours, partial steps are also expected to yield more consistent vorticity dynamics, as discussed in section 6. Note that $|w|$ and $|w'|$ are not significantly modified by the change of momentum advection schemes (not shown).

To sum up at this point, the use of EEN and partial steps improves the model solution at all depths, enhances subsurface mean and eddy flows beneficially, and makes the orientation of the mean flow more physically-consistent with topographic constraints throughout the water column. Eddy-admitting models with reasonable numerics thus seem able to simulate part of the mean circulation driven by eddy-topography interactions, as expected from statistical theories and barotropic potential vorticity arguments. The multi-resolution DRAKKAR model hierarchy would be adequate to further study the impact on these mechanisms of progressive changes of model resolution, as initiated by Merryfield and Scott (2007) from coarse and eddy-resolving solutions.

## 5 Explicit and spurious sidewall friction

A free-slip boundary condition is used in all simulations, except in EENp-ns which differs from EENp only by a no-slip condition. Figures 1, 2, 3, 4, 5, 6, 7 and Table 2 exhibit many changes between EENp and EENp-ns. The barotropic transport at Denmark Straits and the upper global MOC are stronger in EENp than in ENSf and EENf, and further increase by a few percents in EENp-ns. These features are not fully understood yet, but none is due to a stronger Atlantic
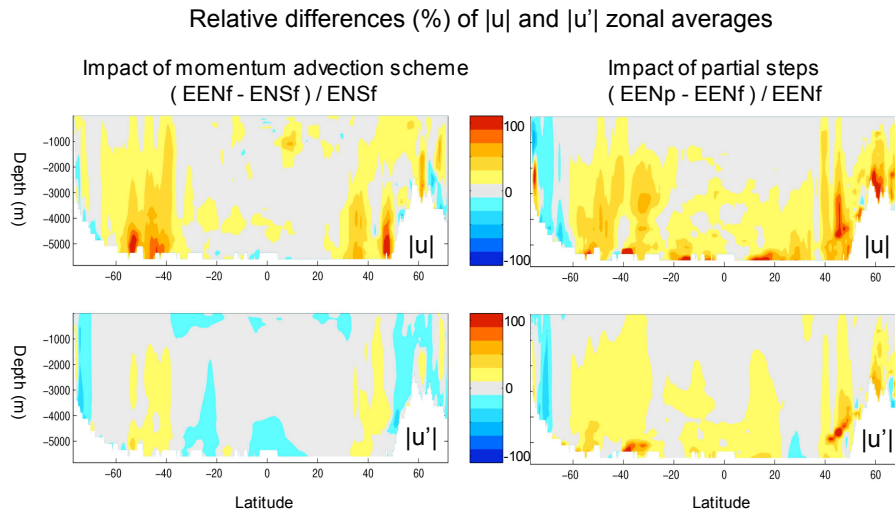
Relative differences (%) of |u| and |u'| zonal averages



**Fig. 8.** Relative differences (%) of $|u|$ (top) and $|u'|$ (bottom) between ENSf and EENf ($100 \times \frac{\text{EENf}-\text{ENSf}}{\text{ENSf}}$, left) and between EENf and EENp ($100 \times \frac{\text{EENp}-\text{EENf}}{\text{EENf}}$, right). $|u|$ and $|u'|$ are the quasi-zonal averages of the time-mean and standard deviation of current intensities, respectively, computed over years 8–10 from each simulation.

upper MOC (which slightly decreases); there is a slight enhancement of the cyclonic circulation around Iceland, and a possible transfer of the overturning circulation at global scale toward the Pacific.

Besides these exceptions, the main impact of the no-slip condition is to bring the EENp solution back towards ENSf or EENf with respect to all remaining features. Indeed, the no-slip condition strongly reduces topostrophy in all local and bottom depth classes (i.e. decorrelates the direction of currents from that of topographic Rossby waves, Fig. 7), weakens the mean and eddy horizontal velocities at depth at all latitudes (not shown), adversely reduces the equatorward excursion of subpolar boundary currents (NRG and Malvinas Current) by about 5°, exagerates the poleward overshoot of subtropical western boundary currents (GS and Brazil Current), widens along-slope currents north of about 50° N as well as the detached GS, makes the path of Agulhas Rings unrealistically straight as in ENSf (see Barnier et al., 2006), strongly reduces the Zapiola Anticyclone transport (see Table 2 and Fig. 4), weakens the Labrador Current, the NAC east of the Grand Banks, most barotropic transports (in Fig. 1b), the DWBC (Figs. 2, 3), and accordingly, the deep overturning circulation (Fig. 1a).

Interestingly, the no-slip condition introduced in EENp-ns cancels out most improvements due to the use of partial steps and/or the EEN scheme. In other words, the side-wall friction brings back the biases diagnosed in ENSf or EENf, most of which were also mentioned in CLIPPER (Penduff et al., 2005) and seen as well in many models at comparable or higher resolutions (Barnier et al., 2006). This strongly support the hypothesis made previously: not using the EEN scheme and partial steps distorts current-

topography interactions and the model solution in free-slip cases (ENSf, EENf, and ENSf-like CLIPPER runs), just as if a numerically-induced spurious sidewall friction was actually present. Adcroft and Marshall (1998) demonstrated the existence of such a spurious sidewall friction within a 1/4°-resolution, C-grid shallow-water idealised model implemented in free-slip with an enstrophy-conserving momentum advection scheme (same numerics as ENSf). Such an effect had been hypothized to explain the absence of the Zapiola anticyclone (De Miranda et al., 1999; Penduff et al., 2001), underestimated sub-thermocline kinetic energy levels and general circulation biases met in CLIPPER with similar numerics (Penduff et al., 2002, 2005) and in other eddy-admitting z-level simulations (Barnier et al., 2006).

Our results thus confirm the existence of spurious side-wall friction in CLIPPER-like models (and presumably other eddy-admitting models), illustrate its adverse impacts on near-bottom flows, along-slope currents at all vertical levels and subsequent realism of numerical solutions up to the surface, and show that these problems are substantially reduced by the use of EEN and partial steps.

The 1/4° OCCAM global model (Coward and de Cuevas, 2005) shares the same resolution and the use of partial steps with EENp. However OCCAM is based on the B-grid MOM3 code (DRAKKAR is based on the C-grid NEMO code), uses an explicit no-slip sidewall friction (vs. free-slip in EENp), a momentum advection scheme in flux form (vs. vector-invariant), and a different pressure gradient ($\nabla P$) scheme. Despite the use of partial steps, OCCAM compares much better with ENSf, EENf or EENp-ns, than with EENp (Barnier et al., 2006). In particular, OCCAM does not simulate the Zapiola Anticyclone. A sensitivity expemiment
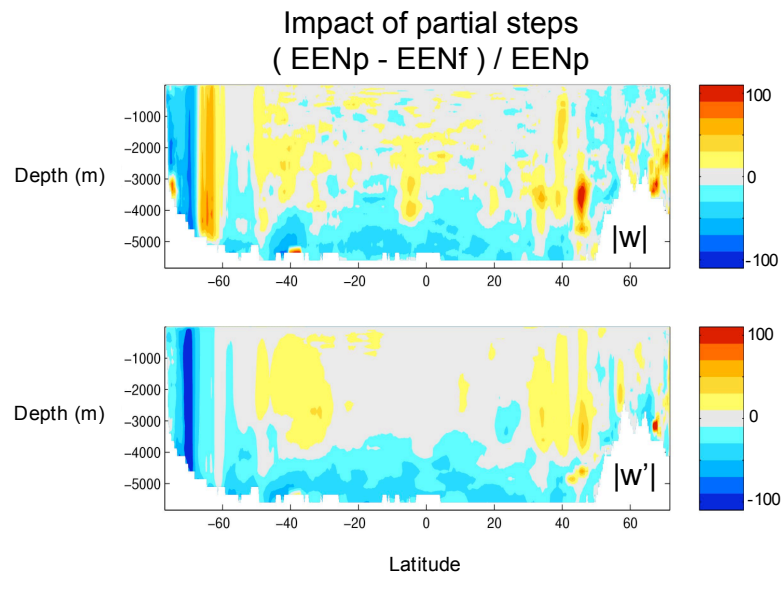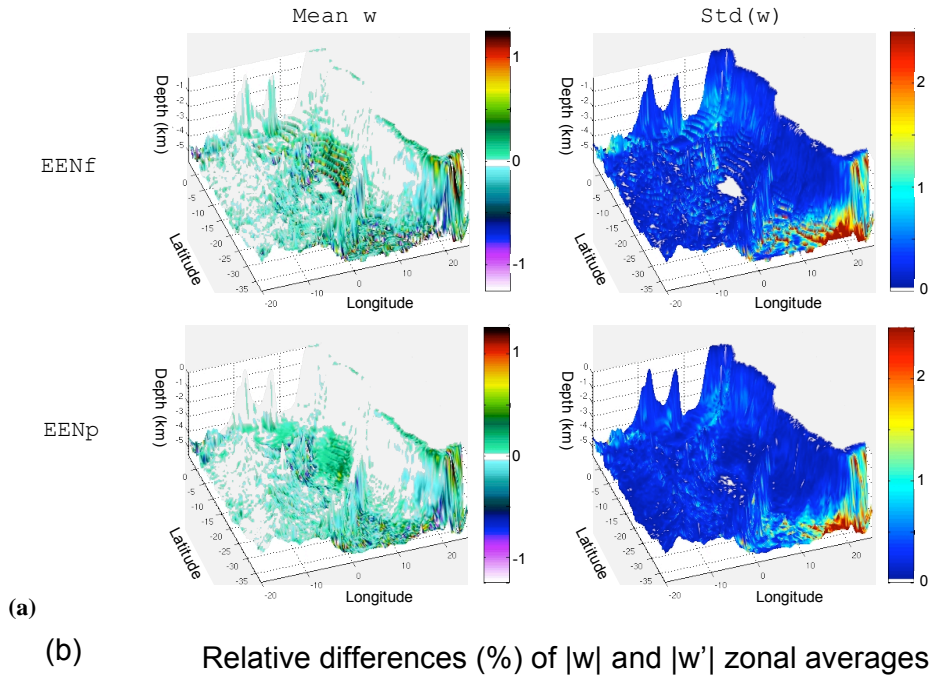
(a)   Cape Basin: mean and standard deviation of vertical velocity (10⁻⁴ m.s⁻¹)



(b)   Relative differences (%) of |w| and |w'| zonal averages



**Fig. 9.** **(a)** Perspective views of bottom vertical velocity statistics ($10^{-4}\ \mathrm{m\,s^{-1}}$) in the Cape Basin from years 8–10. Temporal average of $w$ ($|w|$, left) and standard deviation of $w$ ($|w'|$, right) in simulation EENf (top) and EENp (bottom) . **(b)** Relative differences (%) of $|w|$ (top) and $|w'|$ (bottom) between EENf and EENp ($100 \times \frac{\mathrm{EENp-EENf}}{\mathrm{EENf}}$) computed from years 8–10.

was performed in DRAKKAR, where the EENp model was run with the same $\nabla P$ scheme as OCCAM's. This did not change the solution, nor affected the Zapiola Anticyclone. The explicit no-slip boundary condition used in the OCCAM run (and in most MOM-based simulations) thus likely explains many discrepancies compared to EENp, with a possi-

ble contribution of the momentum advection scheme written in flux-form (shown to degrade the DRAKKAR solution, as shown in Le Sommer et al., 2007).

The consequences of the spurious "no-slip-like" side-wall friction hypothesized in CLIPPER at 1/6° were much less visible at low latitudes, where local Rossby radii were

properly resolved (Penduff et al., 2005). The OFES global model (Masumoto et al., 2004) is based on MOM, uses partial steps with a no-slip sidewall friction like OCCAM, but simulates a reasonable Zapiola Anticyclone at 1/10° resolution. Both facts suggest that increased resolution reduces the adverse effects of no-slip conditions, either introduced explicitly (e.g. B-grid models like OCCAM or OFES), or spuriously (CLIPPER, ENSf, EENf). This strongly supports Adcroft and Marshall (1998)'s conjecture: "in the limit of both high resolution and very low viscosity, [...] the impact of [spurious form stresses along piecewise-constant coastlines] on the structure of the circulation is likely to be reduced".

# 6 Conclusion and discussion

Four 10-year 1/4° global simulations have been analyzed to estimate the impact of numerical choices on DRAKKAR solutions, and to propose dynamical interpretations. Our analysis extends the study by Barnier et al. (2006) beneath the surface and in terms of current-topography interactions. Starting from CLIPPER-like numerics, two successive changes were shown to substantially improve the model solution: replacing the enstrophy-conserving (ENS) by an energy-enstrophy-conserving (EEN) momentum advection scheme, and the full steps by a partial steps topography. The sensitivity of the model solution to no-slip and free-slip boundary conditions helped identify the dynamical origin of these improvements. Interestingly, the use of either ENS instead of EEN, full steps instead of partial steps, or no-slip instead of free-slip conditions (spurious in CLIPPER and ENSp, see Adcroft and Marshall, 1998, and explicit in EENp-ns) has comparable and adverse consequences:

– it weakens deep overturning cells (northward spreading of AABW), horizontal transports at choke points, and boundary currents (Greenland and Labrador Currents, DWBC, GS, GS's northern recirculation gyre, Zapiola anticyclone, etc.);

– it intensifies the bias diagnosed in CLIPPER (Penduff et al., 2002, 2005), i.e. reduces the eddy and mean kinetic energy levels at depth;

– it adversely affects the realism (path, width, structure, unstable character) of the DWBC and mean currents, especially in eddy-active, topographically-influenced regions (GS and both its recirculation gyres, NAC, Northwest Corner, Brazil and Malvinas Currents, Confluence Region, Agulhas Rings);

– it decreases topostrophy, especially at depth. This reveals a weaker tendancy of mean currents up to the surface to align in the direction of topographic Rossby waves, consistently with weaker eddy-topography interactions. This suggests that eddy-admitting models with

adequate schemes can represent topographic rectification processes, at least partly.

Our results indicate that, like partial steps and sidewall boundary conditions, the influence of momentum advection schemes on the simulated dynamics originate near topography (confirmed in Le Sommer et al., 2007) and yield significantly different solutions up to the surface. In other words, the upper-layer circulation improvements reported by Barnier et al. (2006) are surface signatures of near-bottom numerically-induced changes. Adding an explicit sidewall friction, i.e. no-slip boundary condition, to our "best" EENp configuration actually cancels most benefits of the EEN scheme and partial steps, bringing the solution (EENp-ns) back towards CLIPPER-like standards (ENSf) in all aspects. This shows that many discrepancies found in CLIPPER and DRAKKAR simulations performed with enstrophy-conserving (ENS-like) momentum advection schemes come from a spurious sidewall friction inherent to free-slip conditions (Adcroft and Marshall, 1998). Le Sommer et al. (2007) conclude that compared to the EEN scheme, ENS generates substantially more grid-scale velocity shears along topographies, likely to yield more dissipation of deep momentum through biharmonic viscosity, thus to explain weaker kinetic energy at depth.

The use of partial steps decreases the near-bottom intensity of $|w|$ and $|w'|$ (Fig. 9b) by regularizing topographic slopes (see Fig. 3 in Merryfield and Scott, 2007). However, unlike all other quantities under investigation, neither $|w|$ nor $|w'|$ levels are substantially affected near the bottom by the use of EEN instead of ENS, or by the use of no-slip instead of free-slip. It is thus likely that the sensitivity of the mean and eddy flow to these numerical choices is governed more by their rotational part than their divergent part, which directly determines vertical velocities. If we assume that (both explicit and spurious) sidewall friction has comparable effects on deep flows as mesoscale topographic roughness (see the next paragraph), we may conjecture that switching from ENS to EEN, no-slip to free-slip, or full steps to partial steps improves the representation of vorticity dynamics near topographic slopes, and that this effect reaches up to the surface. Mesoscale topographic roughness was shown in quasigeostrophic (QG) models to remove eddy kinetic energy (EKE) from the barotropic mode, i.e. at depth (Treguier and Hua, 1988; Barnier and Le Provost, 1993), by modifying vertical mode interactions and inhibiting the inverse cascade. Switching from the EEN to the ENS scheme, from partial to full steps, and from free- to no-slip conditions interestingly yield very similar effects on DRAKKAR EKE fields, especially in eddy-active topographically-constrained regions. The use of the ENS scheme, full steps, and no-slip conditions reduce the topographic imprint on the general circulation up to the surface, weaken eddy-driven mean features like the Zapiola anticyclone, and topostrophy at all depths. These full-depth changes in the mean circulation might be

driven by both Reynolds stresses and topographic rectification. The first process matches the conjecture made in the companion numerical study by Le Sommer et al. (2007): "more vigorous bottom-intensified eddy motions [...] can interact with the surface-intensified eddy field, resulting in a modification of the mean flow forcing by the surface eddy field" when switching from ENS to EEN. The improved representation of the topographic potential vorticity field ($\frac{f}{H}$), provided by replacing full steps by partial steps, is likely to promote more consistent topographic eddy rectification, and thus the contribution of the second process mentioned above. More generally, quasi-geostrophic vorticity dynamics and eddy rectification theories seem consistent with most of our findings.

Like mesoscale topographic roughness (Treguier and Hua, 1988; Barnier and Le Provost, 1993), bottom friction was shown to decrease subsurface EKE levels in QG and primitive equation models (Rivière et al., 2004), inhibit the inverse cascade and thus weaken the barotropic flow (Panetta, 1993). The smoothing of mesoscale topographic roughness in an eddy-admitting CLIPPER (i.e. ENSf-like) model, thus subject to spurious sidewall friction, was also shown (Penduff et al., 2002) to enhance the penetration of EKE at deep levels and the topographic imprint on the mean circulation (e.g. the Zapiola anticyclone). In other words, the increase of topographic roughness in CLIPPER had comparable effects on the flow as introducing either (i) spurious sidewall friction by replacing EEN by ENS in DRAKKAR, (ii) explicit sidewall friction via a no-slip condition in DRAKKAR, (iii) or topographic roughness in a QG model. The assumption made above about the comparable effect of sidewall friction and topographic roughness, and our QG (rotational) dynamical hypotheses are thus well supported by previous studies.

A substantial topographic smoothing had been shown by Penduff et al. (2002) to reduce the dynamical biases diagnosed in eddy-admitting z-level models like CLIPPER and the present ENSf setup. The present results show that the spurious near-topography no-slip-like friction highlighted by Adcroft and Marshall (1998) and subsequent circulation biases (also typical of other models) can be largely reduced without removing high-wavenumber bathymetric structures, i.e. by the use of adequate momentum advection schemes and partial steps. EENp numerics are being used in present DRAKKAR simulations and are advised for other eddy-admitting simulations with C-grid z-level models. These spurious effects might not be as problematic at higher resolution; both numerical choices yield realistic results in finer DRAKKAR setups ($\frac{1}{12}°$, see DRAKKAR Group, 2007).

It is interesting to note that this global z-level EENp solution shares substantial similarities with regional sigma-coordinate model solutions (see e.g. Ezer and Mellor, 1997; Penduff et al., 2001; Willebrand et al., 2001), in particular enhanced kinetic energies at depth, a realistic Zapiola anticyclone and an improved Gulf Stream path compared to full-step z-level solutions at similar resolutions. Com-

pared to full steps, sigma coordinates and partial steps do not only provide a more accurate grid-scale representation of gentle topographic slopes, associated $\frac{f}{H}$ fields and ambiant potential vorticity gradients. They also allow a direct communication (through advection, diffusion, pressure gradient computations, etc) between adjacent cells along sloping topographies. Both partial-step and sigma-coordinate models thus yield a more continuous representation of bottom Ekman transport and pumping, known to be largely invloved in eddy-topography interactions (see e.g. Dewar, 1998) and topographic steering of mean currents (see e.g. Arhan et al., 1989). Pressure gradients are everywhere computed on the horizontal in NEMO, including with partial steps above topographic slopes (computation at the shallowest of adjacent bottom T-points) without any vertical extrapolation. No sigma-like pressure gradient truncation error nor hydrostatic inconsistancy may thus contaminate discrete pressure gradient computations in our partial steps simulations.

Current-topography and eddy-topography interactions are crucially involved in the systematic improvement seen up to the surface in the sequence of experiments ENSf-EENf-EENp. This suggests that topography also plays a major role in shaping real ocean circulations, locating major surface currents at their observed position and thus the regions where major air-sea interactions occur. Several studies have shown that the explicit resolution of ocean eddies improves the consistency of processes involved in ocean-atmosphere and physico-biogeochemical interactions: besides their significant impact on the variability of oceanic heat transport (Hall et al., 2004) and ocean-atmosphere coupled variability modes (Hogg et al., 2006), ocean eddies are directly involved in upper-ocean processes, e.g. mixed-layer dynamics (Levy et al., 2005), subduction (Valdivieso da Costa et al., 2005) or post-convective restratification (Chanut et al., 2007). Our results emphasize the importance of physically-consistent representations of deep currents and topographic constraints as well, since they shape the circulation and eddy activity at the surface where air-sea interactions ultimately take place.

# References

Adcroft, A. and Marshall, D.: How slippery are piecewise-constant coastlines in numerical ocean models?, Tellus Series A, 60, 95–108, doi:10.1034/j.1600-0870.1998.00007, 1998.

Arakawa, A. and Lamb, V.: A potential enstrophy and energy conserving scheme for the shallow water equations, Mon. Wea. Rev., 109, 18–36, 1981.

Arhan, M., Colin de Verdire, A., and Mercier, H.: Direct observations of the mean circulation at 48°N in the Atlantic ocean, J. Phys. Oceanogr., **19**, 161–181, 1989.

Arhan, M., Treguier, A.-M., Bourlès, B., and Michel, S.: Diagnosing the annual cycle of the equatorial undercurrent in the Atlantic ocean from a general circulation model, J. Phys. Oceanogr., 36, 1502–1522, 2006.

Barnier, B., Madec, G., Penduff, T., Molines, J.-M., Treguier, A.-M. , Le Sommer, J., Beckmann, A., Biastoch, A., Böning, C., Dengg, J., Derval, C., Durand, E., Gulev, S., Remy, E., Talandier, C., Theetten, C., Maltrud, M., McClean, J., and de Cuevas, B.: Impact of partial steps and momentum advection schemes in a global circulation model at eddy permitting resolution, Ocean Dynam., 56(5-6), 543–567, doi:10.1007/s10236-006-0082-1, 2006.

Barnier, B. and Le Provost, C.: Influence of bottom topography roughness on the jet and inertial recirculation of a mid-latitude gyre, Dyn. Atm. Oceans, 18, 29–65, 1993.

Beismann, J.-O., Käse, R. H., and Lutjeharms, J. R. E.: On the influence of submarine ridges on translation and stability of Agulhas rings, J. Geophys. Res., 104, 7897–7906, doi:10.1029/1998JC900127, 1999.

Berliand, M. and Strokina, T.: Global distribution of the total amount of clouds,. hydrometeorological, Technical report, Hydrometeorology Publishing House, Leningrad, (in Russian), 1980.

Blanke, B. and Delecluse, P.: Variability of the tropical Atlantic ocean simulated by a general circulation model with two different mixed-layer physics, J. Phys. Oceanogr., 23, 1363–1388, 1993.

Chanut, J., Barnier, B., Large, W. G. , Debreu, L., Penduff, T., Molines, J.-M., and Mathiot, P.: Mesoscale eddies in the Labrador Sea and their contribution to convection and re-stratification, J. Phys. Oceanogr., in press, 2007.

Chassignet, E., Arango, H., Dietrich, D., Ezer, T., Ghil, M., Haidvogel, D., Ma, C., Mehra, A., Paiva, A., and Sirkes, Z.: DAMEE-NAB: The base experiments, Dyn. Atmos. Oceans, 32, 155–183, 2000.

Colin de Verdière, A., Mercier, H., and Arhan, M.: Mesoscale variability from the western to the eastern Atlantic along 48°N, J. Phys. Oceanogr., 19, 1149–1170, 1989.

Coward, A. and de Cuevas, B.: The OCCAM 66-level model: model description, physics, initial conditions, and external forcing, Internal document 99, Southampton Oceanography Center, Southampton, UK, 2005.

De Miranda, A., Barnier, B., and Dewar, W.: On the dynamics of the Zapiola anticyclone, J. Geophys. Res., 104, 21137–21149, 1999.

Dengg, J., Beckmann, A., and Gerdes, R.: The Gulf Stream separation problem, *The Warmwatersphere of the North Atlantic Ocean*, W. Krauss, ed., Gebrüder Borntraeger, Berlin, 253–290, 1996.

Dengler, M., Schott, F., Eden, C., Brandt, P., Fisher, J., and Zantopp, R.: Break-up of the Atlantic Deep Western Boundary Current into eddies at 8°S, Nature, 432, 1018–1020, doi:10.1038/nature03134, 2004.

Dewar, W.: Topographic and barotropic transport control by bottom friction, J. Mar. Res. , **56**, 295–328, 1998.

Ducet, N., Le Traon, P.-Y., and Reverdin, G.: Global high-resolution mapping of ocean circulation from TOPEX/Poseidon and ERS-1 and -2, J. Geophys. Res., 105(C8), 19477–19498, 2000.

DRAKKAR Group: Eddy-permitting ocean circulation hindcasts of past decades, Clivar Exchanges, No 42 (vol 12 No 3), 8–10 (Unpublished manuscript), 2007.

DYNAMO Group: Dynamo: Dynamics of North Atlantic models. Simulation and assimilation with high resolution models, Technical report, Ber. Inst. f. Meeresk. Kiel, 294, 1997.

Eden, C. and Böning, C.: Sources of eddy kinetic energy in the Labrador Sea, J. Phys. Oceanogr., 32, 3346–3363, 2002.

Ezer, T. and Mellor, G.L.: Simulations of the Atlantic Ocean with a free surface sigma-coordinate ocean model, J. Geophys. Res.., 102, C7, 15,647–15,657, 1997.

Frolov, S. A., Sutyrin, G. G. , and Ginis, I.: Asymmetry of an equilibrated Gulf Stream–type jet over topographic slope, J. Phys. Oceanogr., 34, 1087–1102, 2004.

Griffies, S. M., Böning, C., Bryan, F.O., Chassignet, E.P., Gerdes, R., Hasumi, H., Hirst, A., Treguier, A.-M., and Webb, D.: Developments in ocean climate modelling, Ocean Modelling, 2, 123–192, 2000.

Hall, N., Barnier, B., Penduff, T., and Molines, J.-M.: Interannual variation of Gulf Stream heat transport in a high resolution model forced by reanalysis data, Clim. Dyn., 23, 341–351, 2004.

Hogg, A., Dewar, W., Killworth, P., and Blundell, J.: Decadal variability of the mid-latitude climate system driven by the ocean circulation, J. Climate, 19, 1149–1166, 2006.

Holloway, G.: Representing topographic stress for large-scale ocean models, J. Phys. Oceanogr., 22, 1033–1046, 1992.

Jourdan, D., Balopoulos, E., Garcia-Fernandez, M., and Maillard, C.: Objective analysis of temperature and salinity historical data set over the mediterranean basin, Technical report, IEEE, 1998.

Joyce, T., Dunworth-Baker, J., Pickart, R., Torres, D., and Waterman, S.: On the Deep Western Boundary Current south of Cape Cod, Deep-Sea Res. II, 52, 615–625, 2005.

Kamenkovich, V. M., Leonov, Y. P., Nechaev, D. A., Byrne, D. A., and Gordon, A. L. : On the influence of bottom topography on the Agulhas eddy, J. Phys. Oceanogr., 26, 892–912, 1996.

Lazier, J. R. N.: Observations in the northwest corner of the North Atlantic Current, J. Phys. Oceanogr., 24, 1449–1463, 1994.

Le Sommer, J., Penduff, T., Theetten, S., Madec, G., and Barnier, B.: How momentum advection schemes influence current-topography interactions at eddy-permitting resolution, Ocean Modelling, in press, 2007.

Levitus, S., Boyer, T., Conkright, M., O'Brian, T., Antonov, J., Stephens, C., Stathopolos, L., Johnson, D., and Gelfeld, R.: World Ocean database 1998, Technical Report NESDID18, NOAA Atlas, 1998.

Lévy, M., Estubier, A., and Madec, G.: Choice of an advection scheme for biogeochemical models, Geophys. Res. Lett., 28, 3725–3728, 2001.

Levy, M., Gavart, M., Memery, L., Caniaux, G., and Paci, A.: A

4D-mesoscale map of the spring bloom in the Northeast Atlantic (POMME experiment): results of a prognostic model, J. Geophys. Res., 110, C07S21, doi:10.1029/2004JC002588, 2005.

Masumoto, Y., Sasaki, H., Kagimoto, T., Komori, N., Ishida, A., Sasai, Y., Miyama, T., Motoi, T., Mitsudera, H., Takahashi, K., Sakuma, H., and Yamagata, T.: A fifty-year eddy-resolving simulation of the World Ocean: Preliminary outcomes of OFES (OGCM for the Earth Simulator). *J. Earth Simulator*, **1**, 35–56, 2004.

Merryfield, W. and Scott, R.: Bathymetric influence on mean currents in two high-resolution near-global ocean models, Ocean Modelling, 16, 1-2, 76-94, doi: 10.1016/j.ocemod.2006.07.005, 2007.

Niiler, P., Maximenko, N., and McWilliams, J.: Dynamically balanced absolute sea dynamically balanced absolute sea level of the Global Ocean derived from near-surface velocity observations, Geophys. Res. Lett., 30 (22), 2164, doi:10.1029/2003GL018628, 2003.

Olson, D., Podesta, G., Evans, R., and Brown, O.: Temporal variations in the separation of Brazil and Malvinas currents, Deep-Sea Res., 35, 1971–1990, 1988.

Pacanowski, R. and Gnanadesikan, A.: Transient response in a z-level ocean model that resolves topography with partial cells, Mon. Wea. Rev., 126, 3248–3270, 1998.

Paiva, A., Hargrove, J., Chassignet, E., and Bleck, R.: Turbulent behavior of a fine mesh (1/12°) numerical simulation of the North Atlantic, J. Mar. Res., 21, 307–320, 1999.

Panetta, R.: Zonal jets in wide baroclinically unstable regions: persistance and scale selection, J. Atmos. Sci., 50, 2073–2106, 1993.

Penduff, T., Barnier, B., Béranger, K., and Verron, J.: Comparison of near-surface mean and eddy flows from two numerical models of the South Atlantic Ocean, J. Geophys. Res., 106, 16, 857–16, 867, 2001.

Penduff, T., Barnier, B., Madec, G., and Molines, J.-M.: On the use of current meter data to assess the realism of ocean model simulations, Ocean Modelling, 11, 399–416, 2005.

Penduff, T., Barnier, B., Verron, J., and Kerbiriou, M.-A.: How topographic smoothing contributes to differentiating the eddy flows simulated by sigma- and z-level models, J. Phys. Oceanogr., 32, 122–137, 2002.

Rhines, P. B.: The dynamics of unsteady currents, in The Sea, Wiley Interscience, NY, vol. 6, 189–318, 1977.

Rivière, P., Treguier, A.-M., and Klein, P.: Effects of bottom friction on nonlinear equilibration of an oceanic baroclinic jet, J. Phys. Oceanogr., 34, 416–432, 2004.

Roberts, M., Marsh, R., New, A., and Wood, R.: An intercomparison of a Bryan-Cox type ocean model and an isopycnic model. Part I: The subpolar gyre and high-latitude processes, J. Phys. Oceanogr., 26, 1495–1527, 1996.

Sadourny, R.: The dynamics of finite-difference models of the shallow-water equations, J. Atmos. Sc., 32, 1975.

Smith, R., Maltrud, M., Bryan, F., and Hecht, M.: Numerical simulation of the North Atlantic Ocean at 1/10°, J. Phys. Oceanogr., 30, 1532–1561, 2000.

Steele, M., Morley, R., and Ermold, W.: PHC: A global ocean hydrography with a high quality Arctic Ocean, J. Climate, 14, 2079–2087, 2001.

Timmermann, A., Goosse, H., Madec, G., Fichefet, T., Ethe, C., and Dulière, V.: On the representation of high latitude processes in the ORCA-LIM global coupled sea-ice ocean model, Ocean Modelling, 8, 175–201, 2005.

Treguier, A. M.: Kinetic energy analysis of an eddy resolving, primitive equation model of the North Atlantic, J. Geophys. Res., 97, No C1, 687–701, 1992.

Treguier, A. M. and Hua, B. L.: Influence of bottom topography on stratified quasi-geostrophic turbulence, Geophys. Astrophys. Fluid Dynamics, 43, 265–305, 1988.

Tréguier, A.-M., Reynaud, T., Pichevin, T., Barnier, B., Molines, J.-M., de Miranda, A., Messager, C., Beismann, J.-O., Madec, G., Grima, N., Imbard, M., and Le Provost, C.: The CLIPPER project: High resolution modelling of the Atlantic, Int. WOCE Newslett, 36, 3–5, 1999.

Treguier, A.-M., Theetten, S., Chassignet, E., Penduff, T., Smith, R., and Talley, L.: The North Atlantic subpolar gyre in four high resolution models, J. Phys. Oceanogr., 35, 757–774, 2005.

Trenberth, K., Olson, J., and Large, W. G.: A global ocean wind stress climatology based on ECMWF analyses, Technical Report NCAR/TN-338+STR, NCAR, 1989.

Valdivieso da Costa, M., Mercier, H., and Tréguier, A.-M.: Effects of the mixed layer time variability on kinematic subduction rate diagnostics, J. Phys. Oceanogr., 35, 427–443, 2005.

Willebrand, J., Barnier, B., Böning, C., Dieterich, C., Killworth, P., Le Provost, C., Jia, Y., Molines, J.-M., and New, A.: Circulation characteristics in three eddy-permitting models of the North Atlantic, Progress in Oceanogr., 48, 123–162, 2001.

Xie, P. and Arkin, P.: Global precipitation: A 17-year monthly analysis based on gauge observations, satellite estimates, and numerical model outputs, Bulletin of the American Meteorological Society, 78, 2539–2558, 1997.